TU Delft

Delft University of Technology

Effect of thermal radiation entropy on the outdoor efficiency limit of single-junction silicon solar cells

Ziar, Hesan

DOI
10.1016/j.solmat.2022.111763

Publication date
2022

Document Version
Final published version

Published in
Solar Energy Materials and Solar Cells

Citation (APA)
Ziar, H. (2022). Effect of thermal radiation entropy on the outdoor efficiency limit of single-junction silicon solar cells. *Solar Energy Materials and Solar Cells*, *242*, Article 111763. https://doi.org/10.1016/j.solmat.2022.111763

Important note
To cite this publication, please use the final published version (if applicable).
Please check the document version above.

Copyright
Other than for strictly personal use, it is not permitted to download, forward or distribute the text or part of it, without the consent of the author(s) and/or copyright holder(s), unless the work is under an open content license such as Creative Commons.

Takedown policy
Please contact us and provide details if you believe this document breaches copyrights.
We will remove access to the work immediately and investigate your claim.

This work is downloaded from Delft University of Technology.
For technical reasons the number of authors shown on this cover page is limited to a maximum of 10.

Solar Energy Materials & Solar Cells 242 (2022) 111763

Contents lists available at ScienceDirect

Solar Energy Materials and Solar Cells

journal homepage: www.elsevier.com/locate/solmat

Effect of thermal radiation entropy on the outdoor efficiency limit of single-junction silicon solar cells

Hesan Ziar

Delft University of Technology, Photovoltaic Materials and Devices Group, Mekelweg 4, 2628CD, Delft, the Netherlands

ARTICLE INFO

Index Terms:
Photovoltaics (PV)
Energy conversion
Efficiency limit
Thermal radiation entropy
Exergy

ABSTRACT

Incoming radiation energy illuminating a solar cell contains a certain amount of entropy, which does not contribute to output electrical work. Entropy has a different spectral distribution from the internal energy of light and consequently affects PV cell performance. Here in this work, we investigate the influence of entropy content of thermally radiated light on the maximum achievable efficiency of single-junction solar cells. We revise the value of the well-known Shockley-Queisser (SQ) limit for various absorber materials and take a deeper look at this effect by re-calculating the efficiency limit of crystalline silicon solar cells considering Meitner-Auger recombination. When considering the entropy content of AM 1.5 standard spectrum, the SQ limit for silicon drops from 33.15% to 30.42%. Further, considering Meitner-Auger recombination and using measured properties of silicon, the efficiency limit lowers to 27.12% from the already established 29.43%. This suggests a 4% thinner silicon absorber, reaching a thickness of ~101 μm; hinting PV industry that a thinner Si wafer can provide the optimum outdoor energy yield. We further show that the entropy content of terrestrial radiation is less in favor of c-Si technology and most in favor of amorphous silicon. In the end, we discuss a few applications of considering entropy of incoming sunlight for photovoltaics, which range from PV device design to PV module tilt optimization and even PV system electrical standards.

1. Introduction

Light, as an electromagnetic wave and flux of photons, contains both energy and entropy. Entropy, a thermodynamic quantity with the unit of $J\,K^{-1}$ represents the unavailability of a system's energy for conversion to work. Since light is the input source of energy for solar photovoltaics (PV) cells, its entropy content influences PV cell's performance.

In early 1900s, Max Planck published sets of equations describing internal energy and entropy content of blackbody radiation [1], respectively as $\boldsymbol{U = k\,[h\nu/(exp(h\nu/k_BT)-1)]}$ and $\boldsymbol{S = k\,[(1 + U/h\nu)ln(1 + U/h\nu) - (U/h\nu)ln(U/h\nu)]}$, where $\boldsymbol{k = c/\lambda^4}$ or $\boldsymbol{k = 2c/\lambda^4}$ for polarized and un-polarized light, respectively. $\boldsymbol{h}$ is Planck constant (J s), $\boldsymbol{\nu}$ is light wave frequency (s^{-1}), $\boldsymbol{k_B}$ is Boltzmann constant ($J\,K^{-1}$), $\boldsymbol{T}$ is absolute temperature (K), $\boldsymbol{c}$ is speed of light ($m\,s^{-1}$), and $\boldsymbol{\lambda}$ is wavelength of light (m).

Considering only the energy content of thermal radiation will lead to maximum efficiency $\boldsymbol{\eta_E = [1-(T_0/T)^4][1-(T_0/T)]}$ for a solar energy converter, which the first term shows how good radiation energy is absorbed while the second term represents how good the absorbed radiation energy can be converted to output energy [2–4]. However, when considering the entropy of light, this equation is not valid anymore. Not all radiation is available for useful work and that introduces the concept of *exergy*. Exergy (also named available energy, exergetic energy, availability, and reversible work in the literature) is the maximum theoretical useful work that can be obtained from a system if brought into thermodynamic equilibrium with its environment utilizing ideal processes in which the system interacts only with its environment [5]. It is also defined as the portion of energy that is entirely convertible into all other forms of energy [6]. A key feature of exergy, unlike internal energy, Gibbs free energy, or entropy, is that it considers features of both system and its environment [7]. Thus, when investigating fundamental limits imposed on PV cells (as system) under outdoor conditions (as environment), exergy can play a role. In 1964, Petela derived equations for exergy of radiation, as the maximum ability to carry out work [8]. He obtained the conversion efficiency of radiation to work as $\boldsymbol{\eta_{EX} = 1-(4/3)(T_0/T)+(1/3)(T_0/T)^4}$, where $\boldsymbol{T_0}$ is the environment temperature that the absorber is in thermal equilibrium with and $\boldsymbol{T}$ is the temperature of the radiating blackbody (K). Fig. 1, indicates how these efficiencies change with respect to T_0/T.

Several researchers obtained the same $\boldsymbol{\eta_{EX}}$ equation after Petela and

E-mail address: h.ziar@tudelft.nl.

https://doi.org/10.1016/j.solmat.2022.111763
Received 20 September 2021; Received in revised form 7 April 2022; Accepted 21 April 2022
Available online 28 April 2022
0927-0248/© 2022 The Author(s). Published by Elsevier B.V. This is an open access article under the CC BY license (http://creativecommons.org/licenses/by/4.0/).

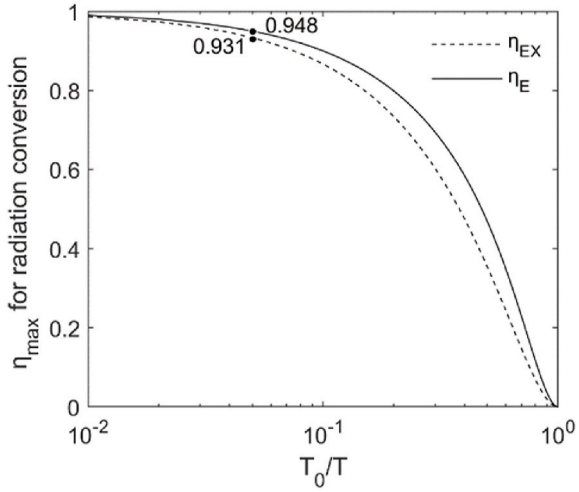

Fig. 1. Maximum conversion efficiency of thermal radiation without (η_E) and with (η_{EX}) considering entropy content of the photons. Points on the graphs show the efficiency values when assuming T_0 = 300 K and T = 5800 K respectively for ambient and radiation temperatures.

the equation is known as Petela efficiency, Landsberg efficiency, or Petela-Press-Landsberg efficiency [8–10]. Further, in 2003, Candau, who obtained the same η_{EX} using classical thermodynamic notions, also derived the monochromatic exergy of radiation as $Ex_\lambda = U_\lambda(T)-U_\lambda(T_0)-T_0[S_\lambda(T)-S_\lambda(T_0)]$ [11]. The equation shows that exergy of radiation can be interpreted as *net entropy-free radiation energy* for a system of emitter-absorber and thereby considers the effect of background ambient radiation. In contrast to energy and entropy, exergy depends on the temperature of both emitter and ambient. Based on this radiative exergy definition, in 2009, Chu and Liu computed the exergy of extra-terrestrial and terrestrial solar radiations and defined the quality of spectral radiation as Ex_λ/U_λ [12]. This means the exergy of radiation is the portion of thermally radiated light that can be used by a converter. In the series of such publications that studied the effect of entropy on the thermodynamic of radiation energy conversion, the key message is that the useful energy of a photon *in a stream of photons*, is less than the well-known term of $h\nu$, as pointed out by Markvart and Bauer [13]. In 2012, they obtained the abovementioned η_{EX} equation by considering the availability of each photon $< h\nu$. Although there have been ideas and suggestions about intrinsic photon entropy [14], since entropy is a parameter of an ensemble, a single photon, as a particle, might not contain entropy. However, an incoherent stream of photons certainly contains entropy.

Despite several research works conducted on the entropy of thermal radiation, entropy has always been the unseen or the dark side of light [14,15], mainly because of the lack of direct application. However, in 2017, Delgado-Bonal showed how considering entropy influences the maximum efficiency of photosynthesis; how the entropy content of terrestrial radiation can hint at the irreversible processes taking place in the atmosphere; and more interestingly how the entropy of radiation played a role in the evolution of human eyesight [15]. No doubt that another research field in which the entropy content of radiation can play a role is photovoltaics.

The conversion efficiency of a photovoltaic device can be obtained either through a statistical balancing of extracted carriers with generated and recombined carriers or by a thermodynamic argument involving energy and entropy balance, in which both approaches are equivalent [16]. The maximum conversion efficiency of photovoltaic devices has always drawn the attention of researchers, starting from the work of Shockley and Queisser in 1961, who showed through a detailed limit approach that the conversion efficiency of p-n junction solar cells can reach up to 33.4% (SQ limit) [17]. Since detailed balancing of incident and generated power densities ignores the non-radiative recombination mechanisms, SQ limit is not well-tuned for indirect band gap semiconductor materials such as silicon (reference [3] chapter 10.2.3), which consist of 95% of produced PV cells [18]. Regarding this information, several researchers worked on the silicon-based PV cell's efficiency limit. In 1984, Tiedje et al. [19] calculated the limiting efficiency as 29.8% showing that non-radiative Meitner-Auger[1] [20–23] recombination is the dominant intrinsic loss mechanism for crystalline Si cells. Then in 2003, Kerr et al. calculated the limit by considering the probability of Meitner-Auger recombination enhancement as a result of increasing carriers density (coulomb-enhanced Meitner-Auger recombination) and reported 29.05% [24]. Further, in 2013, Richter et al. included the most updated standard, measured data, and parameterization knowledge, while including band gap narrowing and reassessed the limit as 29.43% [25], which is currently referred to as the c-Si efficiency limit.

Such solar cell limiting efficiency studies, besides sketching a horizon for c-Si technology, gives hints to the PV industry about designing the best-performing solar cells. For instance, the optimum thickness of the absorber is reported as 90 μm in the work of Kerr et al. [24] while Richter et al. [25] suggested 110 μm. This is due to different physical phenomena considered in their works, among others. Now a question can be raised: does considering thermal radiation entropy yield different efficiency limits and subsequently lead to different optimum design criteria for the PV cells and systems? This research aims to shed light on this question. To answer, first in Section 2 we obtain the SQ limit for various single-junction PV cell materials. Then in Section 3, we calculate the efficiency limit of crystalline silicon PV cells considering the intrinsic properties of silicon and entropy of thermal radiation. Further in Section 4, we discuss the implications of the obtained results and consider a few applications.

2. Methodology

Because of its entropy, a part of sunlight's internal energy is not useable for a PV cell, which is a two-step converter: the radiative energy of photons is first converted to the chemical energy of electron-hole pairs and then converted to electrical energy [3]. In the first conversion step, the generation of charge carriers happens and in the second step, recombination happens. Therefore, we can conclude that the incoming radiation entropy must show its effect on the charge carrier generation rather than recombination. As a result, the exergy of light, instead of its internal energy, contributes to carrier generation in a PV cell. Therefore, we must first calculate the appropriate availability or exergy of the incoming light spectrum. Then, we feed this exergy spectrum into the carrier generation equation. Finally, we obtain the amount of carrier recombination and statistically balance the extraction of carriers with carrier generation and recombination. That enables us to obtain the PV cell ***J-V*** curve and its maximum power point (and other relevant parameters). Ultimately, we compare this electrical work with the internal energy of incoming sunlight in order to obtain the efficiency of PV cell.[2] We do this first without and then with considering Meitner-Auger recombination. In our calculations, we assume that solar cells yield entropy-free electrical energy.

We must note that light as an ensemble of photons contains entropy

[1] *When energy of electron-hole recombination is lost to a third carrier which is excited to a higher energy level without moving to another energy band. For the attribution (Meitner-Auger), this paper followed the suggestions of Richard Sietmann (paper: False attribution, a female physicist's fate, in 1988) and Demetrios Matsakis* et al. *(A renaming proposal: "The Auger–Meitner effect" in 2019), who recommend adding Meitner's name as she discovered the effect one year earlier while Auger extensively investigated it.*

[2] *In thermodynamics, output work divided by total input internal energy is called 1st law efficiency.*

when entering a PV cell as well as when it leaves the cell. When entropy is removed from a converter, its efficiency can increase, however in this work, we neglect the amount of entropy that is removed by spontaneously radiated photos (as a result of carrier recombination) for two reasons: (i) to the author's knowledge, the entropy expression of non-thermally radiated light is only valid inside a cavity [26], and (ii) for silicon, which is the material of interest in this study, radiative recombination has the minor share and thereby photons containing entropy that leave the PV cell are much less than the total number of recombined electron-hole carriers. We also note that entropy reduction of the PV cell by the thermally emitted-out photons does not contribute to carrier recombination statistics and therefore does not need to be considered in carrier statistical balancing.

2.1. Exergy of incoming radiation

First, we consider blackbody radiation and standard AM1.5 spectra as inputs to a p-n junction solar cell and obtain their exergy spectra using the equations by Planck and Chandau reported in Section 1. The standard spectrum used in PV research is AM 1.5 reported in ASTMG173-03 [27]. This spectrum is divided into the beam and diffuse spectra that can be obtained from SMARTS software [28]. Spectral radiation exergy flux (W m^{-2} nm^{-1}) for blackbody, beam, diffuse, and global components are:

$$Ex_{\lambda}^{0} = \Delta\Omega \cos\theta_n \left[U_{\lambda}^{0}(T_e) - U_{\lambda}^{0}(T_a) - T_a\left[S_{\lambda}\left(U_{\lambda}^{0}(T_e)\right) - S_{\lambda}\left(U_{\lambda}^{0}(T_a)\right)\right]\right] \quad (1)$$

$$Ex_{\lambda}^{b} = \Delta\Omega \cos\theta_n \left[U_{\lambda}^{b}(T_e) - U_{\lambda}^{0}(T_a) - T_a\left[S_{\lambda}\left(U_{\lambda}^{b}(T_e)\right) - S_{\lambda}\left(U_{\lambda}^{0}(T_a)\right)\right]\right] \quad (2)$$

$$Ex_{\lambda}^{d} = \pi \left[U_{\lambda}^{d}(T_e) - U_{\lambda}^{0}(T_a) - T_a\left[S_{\lambda}\left(U_{\lambda}^{d}(T_e)\right) - S_{\lambda}\left(U_{\lambda}^{0}(T_a)\right)\right]\right] \quad (3)$$

$$Ex_{\lambda}^{g} = Ex_{\lambda}^{b} + Ex_{\lambda}^{d} \quad (4)$$

where $U_{\lambda}(T)$ and $S_{\lambda}(U_{\lambda}(T))$ are the spectral radiative intensity of energy and its associated entropy (W m^{-2} nm^{-1} sr^{-1}) at temperature T, respectively. Superscripts 0, b, d, and g respectively represent blackbody, beam AM1.5, diffuse AM1.5, and global AM1.5 radiations. Subscripts e and a represent emitter and ambient temperatures. $\Delta\Omega$ is the solid angle to the Sun disc from Earth equals $(Radious_{Sun}/Distance_{Sun\text{-}Earth})^2$. θ_n is the angle of incidence on the sunlight collecting surface. The coefficient π in equation (3) is representative of assuming isotropic hemispherical distribution for the diffuse component of sunlight. We notice that radiation exergy flux from equations (1)–(4) depends only on the spectral distribution of the radiating flux, radiation and environment temperatures, and the geometry between the radiator and the absorber.

2.2. Shockley-Queisser limit considering radiation exergy

Now that we can calculate the exergy of blackbody radiation and AM1.5 global spectra, we can use them as inputs into the SQ limit calculation procedure, clearly explained by Rühle [29]:

$$J_{SC}(E_g) = \int_0^{\infty} A_{bb}(E)\Phi_{Ex}^{i}(E)dE \quad (5)$$

where J_{SC} is the maximum photo-current density (A m^{-2}) which happens at short-circuit conditions. $E_g = hc/\lambda_g$ is band gap energy (eV). $\Phi_{Ex}^{i} = (q\lambda/hc)Ex_{\lambda}^{i}$ is spectral photon flux exergy (C m^{-2} s^{-1}). Superscript i denotes the type of radiation (e.g. blackbody or AM1.5 g). $A_{bb}(E)$ is the ideal absorptance coefficient for band-to-band transition equal to $H(\lambda)$-$H(\lambda$-$\lambda_g)$, where H denotes the Heaviside step function. q is the elementary charge (C). Not all the photo-generated current can reach the PV cell terminals as a result of recombination. To account for that, radiative recombination current density can be calculated as a function of photon energy (E) and externally applied voltage (V) corresponding to quasi-Fermi level splitting (quasi-Fermi levels assumed flat) [26, 29–31]:

$$J_r(E,V) = 2\pi f_g q \int_0^{\infty} A_{bb}(E)\frac{E^2}{h^3c^2\left[e^{E-qV/k_BT_C}-1\right]}dE \quad (6)$$

where T_C is solar cell temperature (K) and f_g is the geometrical factor which is either 1 or 2, respectively when one or both sides of the solar cell emit radiation. A perfect reflector at the solar cell rear side ($f_g = 1$) can slightly increase the efficiency, however, we follow the same assumption as Shockley and Queisser and consider $f_g = 2$.

Then, the output current density J of the solar cell can be written as:

$$J = J_{SC}(E) - J_r(E,V) \quad (7)$$

This equation describes the current-voltage characteristics of the solar cell from which other relevant parameters of voltage at open circuit $V_{OC} = V|_{min|J(V)|}$, voltage at maximum power point $d(JV)/dJ|_{V=Vmpp} = 0$, current at maximum power point $J_{mpp} = J_{SC} - J_r(V{=}V_{mpp})$, maximum power point $P_{mpp} = J_{mpp}V_{mpp}$, and fill factor $FF = P_{mpp}/V_{OC}J_{SC}$. Finally, efficiency is obtained by dividing the maximum power point by spectral photon flux energy of incoming radiation: $\eta_{EX} = P_{mpp}/\Phi_U^i$, where $\Phi_U^i = (q\lambda/hc)U_{\lambda}^{i}$.

2.3. Including Meitner-Auger recombination

So far it was assumed that only radiative recombination happens in the solar cell. However, for indirect materials, such as c-Si, non-radiative Meitner-Auger recombination [20,21] is the dominant current density loss mechanism [32,33]. Therefore, now we extend the calculations to include Meitner-Auger non-radiative recombination. On top of that, free carrier absorption (FCA), measured optical properties of silicon as the absorber, incomplete ionizations, photon recycling, and band gap narrowing (BGN) are also included to have a comprehensive and more accurate limit for single-junction silicon solar cells. As our focus is on the intrinsic properties of silicon, we assume that the solar cell has no surface and defect recombination's and is equipped with a perfect front anti-reflective coating and a perfect back reflector. These assumptions are aligned with previous studies [19,24,25,34]. We follow a similar approach to Richter et al. [25]. We can rewrite equation (7) as:

$$J = J_{SC} - qR_{intr}W \quad (8)$$

where $R_{intr} = \Delta n/\tau_{intr}$ is intrinsic carrier recombination rate (radiative + Meitner-Auger) and W is solar cell thickness, respectively with the units of cm^{-3} s^{-1} and cm. R_{intr} represents how many carriers are recombined per volume in time and it is related to excess carrier concentration Δn and lifetime of carriers in silicon bulk τ_{intr}. To obtain Δn, the solar cell should be modeled as a semiconductor device. In a thorough semiconductor device modeling, parameters are functions of position x in semiconductor length. However, equation (8) assumes a uniform carrier generation and recombination across the solar cell. This implies that quasi-fermi levels are fixed across the solar cell. This is a fair assumption as long as the thickness of solar cell base W_B (positively lowly doped region in an n-type solar cell and vice versa) is smaller than diffusion length of minority carriers L_B (average distance a minority carrier can travel before recombining with a majority carrier), which is known as the narrow-base assumption ($W_B \ll L_B$) of Green [33]. Now we will use this assumption (also used by Richter et al. [25]) and apply the 1-dimensional calculation procedure described by Mcintosh and Altermatt [35], which considers band gap narrowing with Fermi-Dirac statistics.

Let us consider a constant doping profile across the solar cell $N_{dop} = N_D - N_A$, where N_D and N_A are the density of donor (e.g. phosphorous) and acceptor (e.g. Boron) atoms, respectively (cm^{-3}). We describe the

equations for the case of n-doped silicon. Equivalent equations can be applied for p-doped silicon.

As the dopant density increases incomplete ionization increases, however, there is a peak of ~25% near $N_{dop} = 10^{-18}$, as had been suggested by Pearson and Bardeen in 1949 [36] and demonstrated experimentally by Altermatt et al., in 2006 [37]. Although the maximum efficiency happens in low dopant densities [19,24,25], it is interesting to see the effect on the efficiency in other dopant regions.

The majority carrier density at equilibrium is determined by $n_0 = N_D - N_A = N_{dop}$ which is used as the initial value for the majority and minority carrier densities: $n = N_{dop}$ and $p = n_{i0}^2/N_{dop}$, where n_{i0} is the intrinsic carrier concentration of silicon depending on three fundamental parameters of silicon: band gap energy as the difference between conduction and valence bands energy $E_{g0} = E_{C0} - E_{V0}$, the density of states at valence and conduction bands N_V and N_C. These parameters are linked via $n_{i0}^2 = N_V N_C \exp(E_{g0}/k_B T)$. We considered 3.11×10^{19} cm^{-3} and 2.86×10^{19} cm^{-3} for N_V and N_C at 298.15 K, respectively.

The initial values correspond to the silicon being in equilibrium with no BGN and degeneracy ($\gamma_{BGN} = \gamma_{deg} = 1$). Then we use n, p, N_D, and N_A to calculate the density of ionized donors and acceptors, respectively N_D^+ and N_A^-. We applied equations (2), (4), (6) and (7) with Table III parameters from the work of Altermatt et al. [38] to obtain N_D^+ and N_A^-. Now we use N_D^+ and N_A^- instead of N_D and N_A in the rest of the calculations. We recalculate our initial values as $n_0 = N_D^+ - N_A^- = N_{dop}^+$ and $n = N_{dop}^+$ and $p = n_{i0}^2/N_{dop}^+$. Having n and p, then valence and conduction bands shifts ΔE_V and ΔE_C along with band gap narrowing $\Delta E_g = \Delta E_C - \Delta E_V$ are calculated using Schenk's model [39]. It is recommended to use Appendix A of McIntosh and Altermatt 2010 paper [35] when implementing Schenk's model.

Altermatt et al. demonstrated in 2002 [40] that when doping level increases, Fermi-Dirac statistics should be used instead of Boltzmann statistics. Here, Fermi-Dirac statistics are used for majority carrier concentration and Boltzmann statistics for minority carrier concentration. With Fermi-Dirac statistics we have:

$$n = N_C F_{1/2}\left(-\frac{E_C - E_{fn}}{k_B T}\right) \tag{9}$$

$$p = N_V F_{1/2}\left(-\frac{E_{fp} - E_V}{k_B T}\right) \tag{10}$$

where $F_{1/2}$ is ordered 1/2 of the Fermi-Dirac function [41]. In the case of Boltzmann statistics, $F_{1/2}$ is replaced by an exponential function. E_{fn} and E_{fp} are respectively electron and hole Fermi levels while $E_V = E_{V0} - \Delta E_V$ and $E_C = E_{C0} - \Delta E_C$. Assuming n-type silicon and combining equations (9) and (10), we have:

$$np = n_{i0}^2\, \gamma_{\deg}\, \gamma_{BGN} \exp\left(-\frac{E_{fp} - E_{fn}}{k_B T}\right) \tag{11}$$

$$\gamma_{\deg} = F_{1/2}\left(-\frac{E_{C0} - E_{fn}}{k_B T}\right) \Big/ \exp\left(-\frac{E_{C0} - E_{fn}}{k_B T}\right) \tag{12}$$

$$\gamma_{BGN} = \exp\left(\frac{\Delta E_V}{k_B T}\right) \frac{F_{1/2}\left(-\frac{E_C - E_{fn}}{k_B T}\right)}{F_{1/2}\left(-\frac{E_{C0} - E_{fn}}{k_B T}\right)} \tag{13}$$

$\gamma_{deg} \leq 1$ and is a ratio function representing the difference between Fermi-Dirac and Boltzmann statistics. It decreases from unity when carrier concentration increases. On the other hand, $\gamma_{BGN} \geq 1$ increases when carrier concentration increases. γ_{BGN} represents the influence of the narrowed band gap. At equilibrium: $E_{fn} = E_{fp} = E_f$ and thus: $n_0 p_0 = n_{i0}^2 \gamma_{deg} \gamma_{BGN}$. Now one can apply inverse Fermi function on equation (9) and obtain: $-(E_C - E_{fn})/k_B T = F_{1/2}^{-1}(n/N_C)$ and $-(E_{C0} - E_{fn})/k_B T = F_{1/2}^{-1}(n/N_C) - \Delta E_C/k_B T$. As n, N_C, ΔE_C are known from previous steps, γ_{deg} and γ_{BGN} can then be obtained. For inverse 1/2 order of Fermi function, $F_{1/2}^{-1}(u) \approx \ln(u/(1-u/4))$ is used as approximation [42,43]. Finally, minority carrier concentration at equilibrium is calculated by $p_0 = n_0 p_0 / N_{dop}^+$. At this point, one can use minority carrier current and continuity equations to calculate Δn [35]. However, equation (8) implies a narrow-base assumption, also for the sake of speed and simplicity of calculations, the following equation which is based on a narrow base assumption was used [25]:

$$np = (n_0 + \Delta n)(p_0 + \Delta n) = n_{i0}^2 \exp\left(\frac{\Delta Eg}{k_B T}\right) \exp\left(\frac{qV}{k_B T}\right) \tag{14}$$

where $n_{i0} \exp(\Delta E_g/2k_B T)$ is known as effective carrier concentration $n_{i,eff}$. Equation (14) assumes ideal contacts to collect charge carriers which means that quasi-Fermi level separation is equal to the applied voltage, and thus Δn can be obtained as a function of voltage. Finally, n and p are calculated through $n = n_0 + \Delta n$ and $p = p_0 + \Delta n$.

Further, we continue with calculating τ_{intr} using the parametrization developed by Richter et al., in 2012 (equations (18) and (19) in Ref. [44]). The parametrization includes radiative and Coulomb-enhanced Meitner-Auger recombination and has a general form of $\tau_{intr} = \Delta n/[(np - n_{i,eff}^2)(C_{n0} g_{eeh} n_0 + C_{p0} g_{ehh} p_0 + C_{\Delta n} \Delta n^{0.92} + B(1 - P_{PR}))]$. C_{n0}, C_{p0}, and $C_{\Delta n}$ are constants while g_{eeh} and g_{ehh} are functions representing procedures in which respectively electron and hole act as the third carrier in Meitner-Auger recombination. B is the rate of radiative recombination and can be expressed as $B_{rel} \times B_{low}(T)$ where $B_{low}(T) = \int B(E,T) dE$ is the radiative recombination coefficient at temperature T for lowly doped silicon formulated by Trupke et al., in 2003 [45] and B_{rel} is a relative injection-dependent coefficient developed by Altermatt et al., 2005 [46]. $B(E,T)$ is written as:

$$B(E,T) = \frac{1}{\pi^2 c^2 \hbar^3 n_{i,eff}^2} n_r^2(E) E^2 \alpha_{bb}(E) \exp\left(-\frac{E}{k_B T}\right) \tag{15}$$

where α_{bb} is the absorption coefficient for band-to-band transition and n_r is the refractive index of silicon, both obtained from Green's table of self-consistent optical parameters of intrinsic silicon published in 2008 [47]. $\hbar = h/2\pi$ is reduced Planck's constant. $P_{PR} = \int A_{bb}(E) B(E,T) dE / \int B(E,T) dE$ is the probability of photon recycling after radiative recombination. It is worth noting that the internal luminescent light as a result of carriers recombination was assumed to be entropy-free because photon recycling already has a small effect on solar cell efficiency and to the author's knowledge, the entropy expression of non-thermally radiated light is only valid inside a cavity [26]. So far, we have all the ingredients to calculate R_{intr}. The only remaining parameter is A_{bb}. In Section 2.2, A_{bb} was formulated ideally using the Heaviside step function, however, in this section it is defined as:

$$A_{bb}(E) = \frac{\alpha_{bb}(E)}{\alpha_{bb}(E) + \alpha_{FCA}(E) + \frac{1}{4n_r^2 W}} \tag{16}$$

where α_{FCA} is a coefficient representing free carrier absorption. To calculate α_{FCA} Rüdiger's parametrization of free carrier absorption published in 2013 is used [48]. Considering the randomized light-trapping scheme and the isotropic response of the solar cell, the mean path of a light ray inside of the solar cell equals $4n_r^2 W$. The chance for creating multiple electron-hole pairs by high energy photons is neglected in equation (16) because this effect has a minor contribution of <0.1 mA/cm^2 [34,49]. Having equation (16) in hand, A_{bb} is plugged into equation (8) to calculate J_{SC} as well. Further, J-V characteristics of the solar cell and finally the parameters of interest can be obtained in analogy to Section 2.2.

For graphs and visualization purposes, resistivity ρ of the doped silicon is also calculated using Arora et al. model [50] of carrier mobility μ and applying $1/\rho = q(n\mu_e + p\mu_h)$. Here, n and p are obtained while neglecting incomplete ionization since dopant atoms contribute to resistivity if they substitute silicon atoms in the lattice, regardless of ionization (substitutional concentration). As n and p are both functions of cell voltage, depending on the graphs, ρ was calculated at

short-circuit, maximum power point, and open-circuit.

To identify the validity area of narrow base assumption in the graphs, minority carrier diffusion length $\boldsymbol{L}$ was calculated and compared with silicon thickness assuming $\boldsymbol{W_B \approx W}$, using $\boldsymbol{L = (D\tau)^{1/2}}$, where the diffusion coefficient is $\boldsymbol{D = \mu k_B T/q}$. For n-type silicon, hole mobility was used, as well as for p-type silicon mobility of electrons. As **L** is a function of excess carrier concentration $\boldsymbol{\Delta n}$ through $\boldsymbol{\tau}$, and $\boldsymbol{\Delta n = 0}$ at short-circuit, $\boldsymbol{L}$ was only calculated at maximum power point and open circuit.

3. Results

3.1. Exergy of incoming radiation

We start with calculating thermal radiation exergy using Planck's formulation for energy and entropy (refer to Section 1) and equations (1)–(4). For standard AM1.5, the Sun zenith is 48.236° and the surface tilt is 37° (both with the same azimuth of 180°), therefore the angle of incidence becomes 11.236°. The solid angle to the Sun disc from Earth is calculated as 6.79×10^{-5} sr.

Fig. 2 shows the spectral radiation energy (red) and exergy (blue) fluxes for beam AM 1.5 (AM1.5b), diffuse AM 1.5 (AM1.5d), global AM1.5 (AM1.5 g), and 5800 K blackbody along with their spectral radiation quality. The average quality factor for beam, diffuse, and global AM 1.5, as well as blackbody spectra over 280 nm–4000 nm are 93.39%, 79.04%, 92.01%, and 93.74%, respectively. As can be seen, radiation quality is highest for blackbody radiation and lowest for diffuse radiation. It means that as the sunlight radiation passes through the air and gets diffused, the portion of the photon's internal energy that can be used (exergy) is reduced. This can be attributed to higher disorder of photons and redshift of the energy spectrum. Besides air mass, ambient temperature also influences the exergy of incoming thermal radiation. Fig. 3 quantifies the combined effects of air mass and ambient temperature on the exergy of the beam, diffuse, global terrestrial and blackbody radiation. As can be seen, increasing air mass and temperature reduces the available convertible energy in sunlight. Contour plots show that temperature has the most significant effect on the exergy of diffuse radiation. Note that, since various solar energy converter materials are sensitive to different bandwidths, the effective radiation quality factor varies depending on the material. We will touch upon this topic at the end of the paper where we discuss the applications of considering entropy in the PV industry.

3.2. Shockley-Queisser limit considering radiation exergy

Now using the obtained radiation exergy spectra, we calculate the detailed balance limit through the method explained in Section 2.2. Cell temperature is considered 298.15 K and the efficiency limit is calculated for a band gap range of 0.31 eV–4.42 eV. Fig. 4 represents the efficiency limit with 5800 K blackbody and AM 1.5 g energy and exergy spectra. To check the accuracy of our calculations in this section, $\boldsymbol{\eta_E}$ results were compared with Rühle's published values [29] and were concurrent. As can be seen, using the exergy of radiation as input instead of its internal energy reduces the limit from 33.15% to 30.42% while the optimum band gap remains the same at 1.34 eV. However, for the case of blackbody radiation, the optimum band gap increases very slightly from 1.27 eV to 1.28 eV. This is related to fact that the peak in blackbody energy and entropy happens at different wavelengths. Fig. 4 also includes record lab efficiency values of various PV cell technologies (cell area $\geq$0.99 cm^2), as reported in version 56 of solar cells efficiency tables [51]. Band gap values for each technology are calculated using reported external quantum efficiency (EQE) curves of the cells plotted in various versions of the solar cell table, namely versions 41, 45, 50, 53, 54, and 55 [52–57]. To calculate Eg, $\boldsymbol{EQE|_{(Eg)} = 0.1}$ is applied which is the approach taken by other authors [29], alternatively one can calculate E_g using the condition at which $\boldsymbol{|dEQE/dE_g|}$ is maximized [58]. We note that all the lab efficiencies so far have been below the exergy imposed detailed balance limit (dashed red line). Whether or not the lab efficiency of solar cells can break this limit is discussed in Section 4.

3.3. Including Meitner-Auger recombination

Since the PV industry is dominated by silicon as the key material,

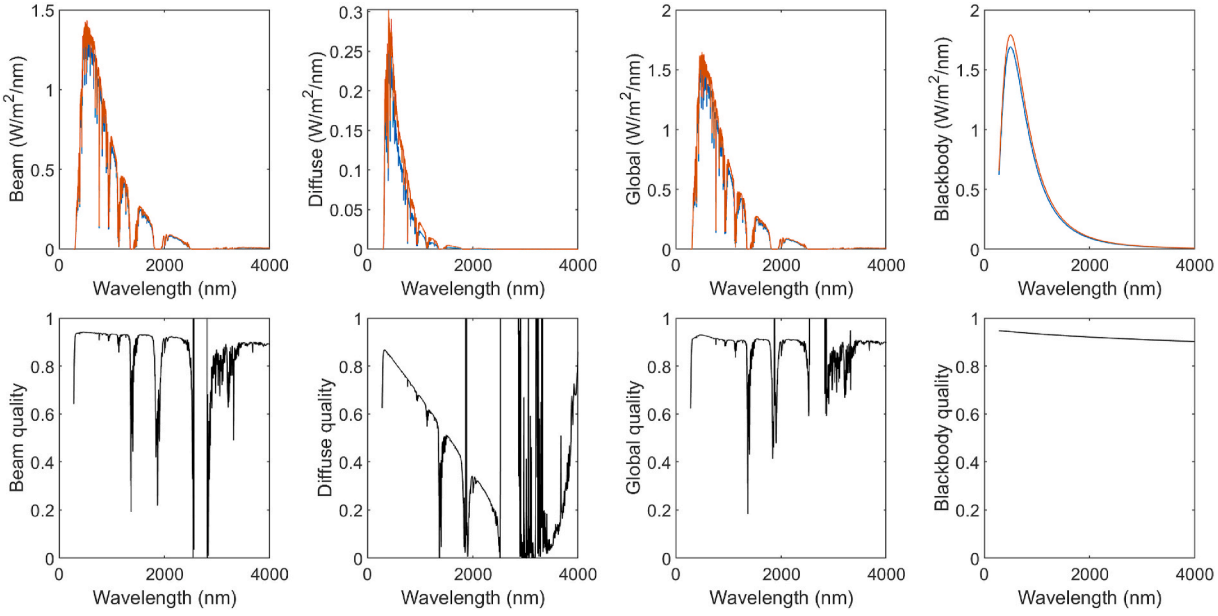

Fig. 2. Top spectral radiation energy (red) and exergy (blue) fluxes respectively from left to right for beam AM 1.5, diffuse AM 1.5, global AM1.5, and blackbody. Energy spectra were obtained using SMARTS 2.9.2 with the standard atmospheric condition. **Bottom**, respectively from left to right: spectral radiation quality, $\boldsymbol{Ex_\lambda/U_\lambda}$, for beam AM 1.5, diffuse AM 1.5, global AM1.5, and blackbody. The calculated quality factors for terrestrial radiations are in close agreement with the work of Chu and Liu [12]. The blackbody radiation energy and exergy were calculated assuming 5800 K and 298.15 K as the emitter and ambient temperatures, respectively. The MATLAB code to extract the exergy of arbitrary thermal radiation is available by submitting a reasonable request to the author. (For interpretation of the references to colour in this figure legend, the reader is referred to the Web version of this article.)

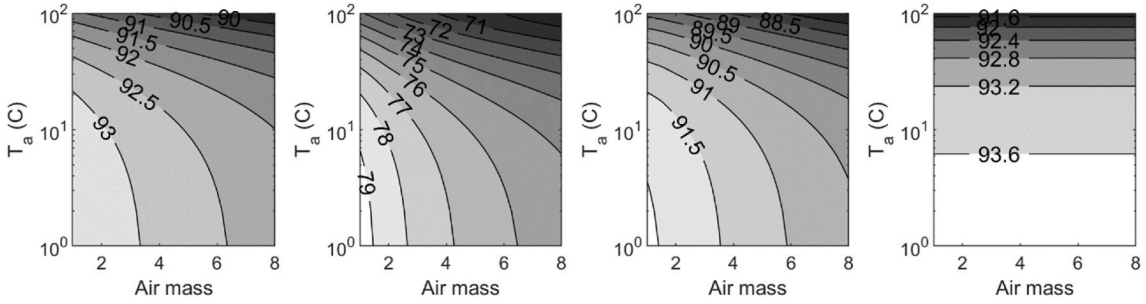

Fig. 3. Radiation exergy as a function of air mass and ambient temperature, respectively from left to right for terrestrial beam, terrestrial diffuse, terrestrial global, and 5800 K blackbody radiations. Blackbody radiation, by definition, disregards air mass, therefore the only influence is temperature. To obtain the plots, first, the energy spectra were calculated using SMARTS 2.9.2 at standard atmospheric conditions. Then all the inputs in SMARTS were kept the same while changing the air mass card from 1 to 8. Further, these spectra were fed into equations (1)–(4) to obtain exergy spectra, while changing the ambient temperature from 0 to 100 Celsius.

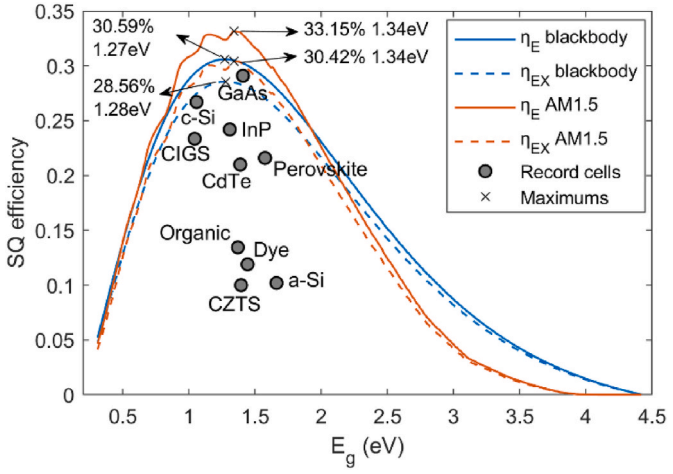

Fig. 4. Detailed balance limit curves as a function of band gap considering energy and exergy of blackbody and AM 1.5 g spectra. It is worth noting that Shockley and Queisser considered blackbody radiation of 6000 K and cell temperature of 300 K, however, here we assumed 5800 K and 298.15 K for radiation and cell temperatures, respectively (closer to Sun's temperature and aligned with standard cell temperature). The MATLAB code to extract a detailed balance limit of arbitrary thermal radiation and band gap range is available by submitting a reasonable request to the author.

next we put the focus on the case of silicon as an absorber material. The procedure and set of equations described in Section 2.3 are applied. For carrier concentration calculation, the obtained values were compared with the output of *pvlighthouse* [59], and a close agreement was found.

We consider several parameters of interest as listed in Table 1 and calculate them with respect to absorber thickness $\boldsymbol{W}$ and dopant density $\boldsymbol{N_{dop}}$. Like Section 3.2, we compare the result considering the photon's internal energy ($\boldsymbol{E}$) and available useable energy ($\boldsymbol{Ex}$), for which AM 1.5 g energy and exergy spectra were used as inputs, respectively. Results are only presented for the case of n-type silicon and one can obtain the result for the case of p-type silicon by applying equations described in Section 2.3 analogous to the p-type semiconductor.

Table 1 shows the values for several parameters at the maximum theoretical efficiency when considering internal and available energy of the incoming thermal radiation. The maximum efficiency happens at the limit of un-doped silicon ($\boldsymbol{N_{dop}} = \boldsymbol{10^{12}}$ cm^{-3}), which is aligned with previous literature reports [19,24,25]. As can be seen, considering the available energy of the streams of photons incident on a silicon solar cell instead of on their internal energy reduces the maximum theoretical efficiency from 29.65% to 27.12%.

As expected, Table 1 shows that current is majorly affected when exergy of radiation is considered, while voltage experiences a small drop of ~1 mV at the open circuit and MPP. It is meanwhile important to notice that the optimum thickness of silicon drops around 4% from 105 to 101 μm (Richter et al. had calculated optimum thickness as ~110 μm [25]). This drops because when the amount of available energy in the light spectrum is less, increasing silicon thickness will not contribute to further absorption and photocurrent generation while the chance for recombination rises. This could be an important note for the silicon PV industry that moving towards thinner wafers is indeed beneficial.

Several other parameters are also listed in Table 1. Values show that 4% incomplete ionization happens at the efficiency limit. Resistivity at the maximum power point is slightly higher (~0.01 Ω cm) for AM 1.5 g exergy because of a slightly lower excess carrier concentration and consequently lower carrier concentration. Results are reliable as the narrow-band assumption remains valid due to large $\boldsymbol{L_{MPP}/W}$ for both energy and exergy related values.

Calculations for the case of AM 1.5 g internal energy are not only done for comparison with the case of exergy but also to make a comparison with the previous works to assess the calculation of the presented results. It is worth mentioning that as band gap narrowing is mainly a function of dopant density and temperature [39], at low dopant densities, BGN is almost negligible (0.045 meV for $\boldsymbol{N_{dop}} = 10^{12}$ cm^{-3}) and thus has negligible impacts on effective carrier concentration (changes $\boldsymbol{n_{i,eff}}$ from 8.2800×10^9 to 8.2873×10^9, ~0.09% increase). Therefore, based on the calculation of the present work, with and without band gap narrowing the maximum theoretical efficiency does not change while efficiency changes for higher dopant densities. This is not in complete agreement with the previous work of Richter et al. [25] who reported a 0.14% absolute drop in maximum theoretical efficiency when considering band gap narrowing. With and without band gap narrowing, Richter had reported respectively 29.57% and 29.43% while this work resulted in both 29.65%. Several attempts by the author failed to identify the source of this deviation. Nevertheless, the closeness of the reported results can be regarded as cross-validation of both calculations, the present and the previous work, especially when considering the contour plots depicted in Fig. 5.

In Fig. 5, the trends of $\boldsymbol{\eta}$, $\boldsymbol{V_{OC}}$, $\boldsymbol{V_{MPP}}$, $\boldsymbol{\Delta n_{MPP}}$, $\boldsymbol{J_{SC}}$, $\boldsymbol{FF}$, τ_{MPP}, and $\boldsymbol{\Delta n_{OC}}$ are plotted with respect to absorber thickness $\boldsymbol{W}$, dopant density $\boldsymbol{N_{dop}}$, and absorber resistively $\boldsymbol{\rho}$. Fig. 5 (a) considers entropy-free AM1.5 g as input radiation while Fig. 5 (b) considers the entropy content of AM1.5 g. The limit for which minority carrier diffusion length $\boldsymbol{L}$ is one order of magnitude larger than the thickness $\boldsymbol{W}$ is depicted with red dash lines ($\boldsymbol{L/W} = \boldsymbol{10}$). Calculated values on the right and above this dashed line are less accurate because the narrow-base assumption is less valid in those regions. Depending on the contour plot parameter, $\boldsymbol{\rho}$ and $\boldsymbol{L}$ are calculated at either SC, MPP, or OC, as described in Section 2.3.

4. Implications and applications

Now that it is shown that the efficiency limit of single-junction

Table 1
Silicon solar cell parameters at the calculated efficiency limit considering internal and available energy of incoming thermally radiated photons.

	η (%)	V_{OC} (mV)	J_{SC} (mA/cm^2)	FF (%)	V_{MPP} (mV)	Δn_{MPP} (cm^{-3})	Δn_{OC} (cm^{-3})	BGN (meV)	N_{dop}^{+} (cm^{-3})	ρ_{MPP} (Ω.cm)	L_{MPP}/W (−)	W (μm)
AM 1.5 g energy (E)	29.65	768.1	43.38	89.00	701.8	7.07×10^{15}	2.57×10^{16}	0.045	9.6×10^{11}	0.4831	34.3	~105
AM 1.5 g exergy (Ex)	27.12	767.2	39.72	88.98	700.8	6.94×10^{15}	2.53×10^{16}	0.045	9.6×10^{11}	0.4926	36.1	~101

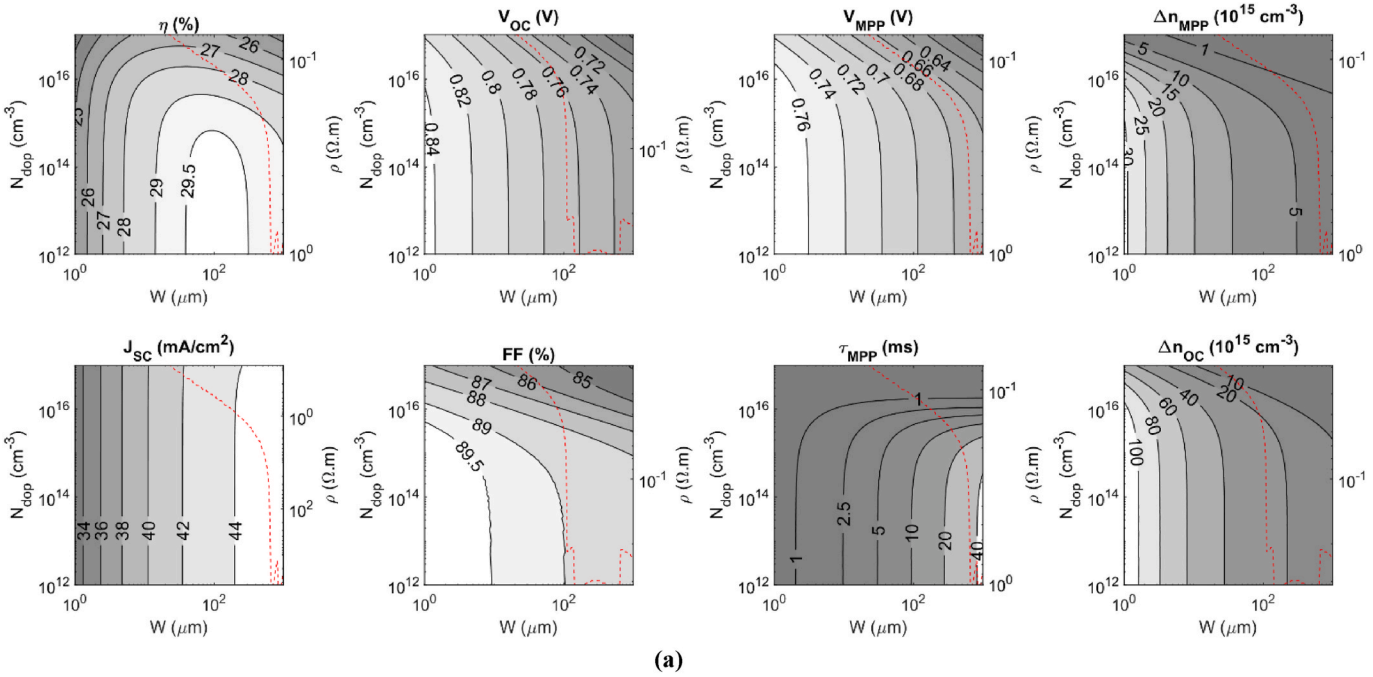

(a)

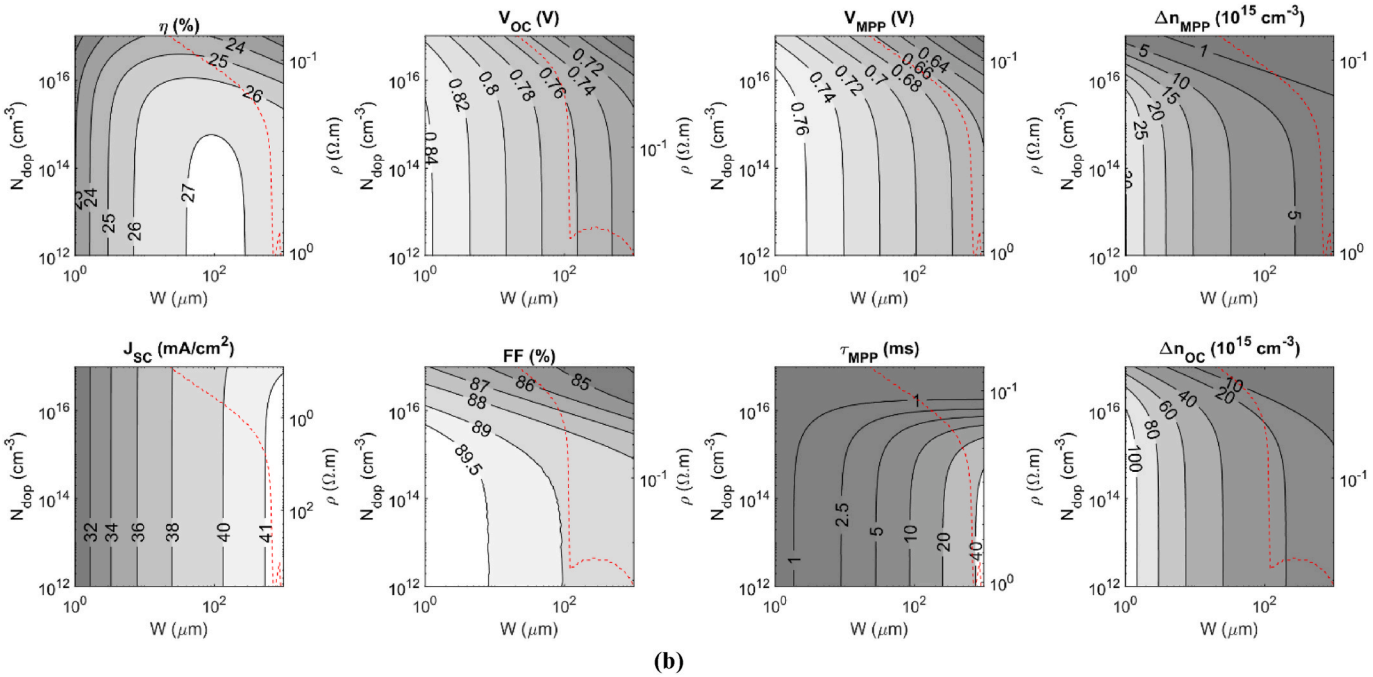

(b)

Fig. 5. Logarithmic contour plots of n-type silicon solar cell parameters with respect to bulk thickness and dopant density, when considering **(a)** energy of AM1.5 g radiation and **(b)** exergy of AM1.5 g radiation. The border for the validity of narrow-band assumption is depicted with red dash lines, where the minority carrier diffusion length is one order of magnitude larger than the base thickness. (For interpretation of the references to colour in this figure legend, the reader is referred to the Web version of this article.)

crystalline silicon solar cells is ~2.5% absolute less than the previously established value, it is worth asking: does understanding this really make a difference? Before answering this question, we must address a discrepancy.

Fig. 4 showed that all the lab record efficiencies were below the η_{EX} limit. However, by looking further into the J_{SC} values of record cells in Fig. 6, we notice that record c-Si has a higher current density than the prediction of the η_{EX} approach. The reported J_{SC} for this record solar cell is 42.65 mA/cm^2 while the calculated J_{SC} based on the exergy of incoming photons is 41.4 mA/cm^2. What is the reason for this discrepancy?

One hypothesis could be neglecting entropy reduction by emitted-out photons. Recombination rate increases by increasing voltage and band gap. In a short circuit, the recombination rate is several orders of magnitude less than the generated current. For instance, for the case of record c-Si cell at Eg = 1.057 eV, the generated current density is 41.4 mA/cm^2 while the recombination current density is 1.15×10^{-12} mA/cm^2. Therefore, the assumption of neglecting the entropy reduction as a result of photons emitted out cannot be the cause of this discrepancy. Another reason could be a slight difference between the interpreted bandgap from the EQE graph and the real Eg. For instance, if the Eg of the recorded cell was ~1.03 eV, both its efficiency and J_{SC} would remain below the limit. Although there might be such a possibility it is not a solid argument to fully address this discrepancy.

The reason for this discrepancy, however, lies behind the way that incoming optical power is *made* and *measured* in laboratories. Collimated light rays are used for testing PV cells [60,61], and solar cell efficiency limits are calculated under the assumption that the incoming optical power is collimated [4]. This means under lab conditions solar cells are facing almost 100% beam irradiance while in real-world conditions diffuse light exists. For instance, STC atmospheric condition leads to ~900 W/m^2 of the beam and ~100 W/m^2 of diffuse light. The overall efficiency of a solar cell is a combination of its beam and diffuse efficiencies: $\eta = f_{beam}\eta_{beam} + \eta_{diffuse}(1\text{-}f_{beam})$, where f_{beam} is the share of the beam's component in optical power [4]. Hence, since the radiation quality factor is different for beam and diffuse irradiances, then the overall efficiency for global light is less than the beam light, and so is the J_{SC}. Considering the above argument, J_{SC} is calculated for a condition

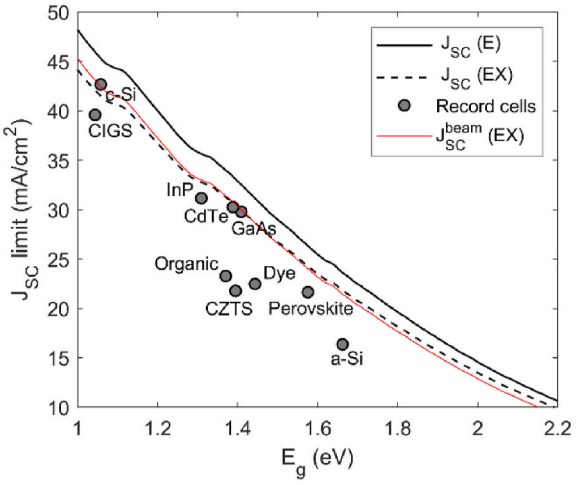

Fig. 6. Limit of short circuit current density as a function of band gap obtained from the detailed balance approach (Section 2.2) which considers internal energy (J_{SC}(E)) and exergy (J_{SC}(Ex)) of incoming radiation. Reported J_{SC} of various record solar cells are also depicted. The red line shows the J_{SC} limit when all the incoming irradiance (1000 W/m^2) is direct. To obtain this, it was assumed that increasing beam irradiance from 900 W/m^2 to 1000 W/m^2 does not influence the share of its entropy content, simply a normalization factor was used. (For interpretation of the references to colour in this figure legend, the reader is referred to the Web version of this article.)

that all the incoming light is direct and depicted with the red curve in Fig. 6. As can be seen, it increases to 42.45 mA/cm^2, a very close number to the J_{SC} of the c-Si record cell (within ±0.5% of the record short circuit current).

The second reason under consideration is as follows. Optical power is usually measured by reading the electrical output signal of calibrated primary, secondary, or working-class sensors, through thermoelectric, photovoltaic, or photoelectric effects, such as thermopile pyranometers, silicon pyranometers, reference cells, or photodiodes [62]. Either way, the number of collected electrons at the terminal of the sensor per unit of time is the measure of optical power. This means that the exergy of photons instead of their internal energy is measured in the lab and solar cells are tested in the lab under a spectrum that its exergy is equivalent to AM1.5 g, not its internal energy.[3] A supporting argument is provided in the footnote [63]. Thus, intentionally or unintentionally most of the calculations in the solar cells industry assume that solar cells are dealing with entropy-free incoming radiation, which works fine if we test and compare PV cells in the lab.[4] We note that the obtained limit may not sustain in a lab environment and there is a possibility that in the near future it breaks by lab record solar cells. However, it remains valid under real-world STC conditions, where the incoming light contains entropy and shares its available energy between direct and diffuse components. Therefore, the obtained limits in this work are better to be addressed as *outdoor terrestrial efficiency limits*.

4.1. Laboratory measurements

As long as PV cells are tested in the lab under the same radiation spectrum whose exergy is AM 1.5 g, a fair comparison can take place. However, for outdoor application, we must notice that the PV cell's true efficiency is actually lower than the certified in-lab efficiency. And this is not only because of the deviation from lab working environments but also because light entropy, as it has spectral dependence, might be more in favor of some PV cell materials than others. This can be identified by calculating the effective radiation quality factor, which is discussed in Section 4.3 and quantified in Table 2.

4.2. PV device simulation and design

As discussed in Section 3.3, considering the entropy of incoming light might lead to a slightly different optimum thickness for the silicon absorber (4% lower). Knowing that absorption and recombination are both volumetric parameters, the thickness threshold for which the total recombination compensates the total carrier generation reduces when the availability of the incoming light decreases. Therefore, the entropy content of incoming light influences the optimum absorber design. If outdoor performance is targeted [64] instead of in-lab efficiency, then PV cell designs can be further optimized considering the entropy content of incoming light. This can eventually lead to saving material costs in PV cell production (e.g. 4% less silicon for real-world STC designs).

4.3. PV system design and tilt optimization

The entropy content of light could impact optimizing the tilt angle of

[3] *Evidence for this argument: if irradiance sensors, that are installed both in the lab and outdoors, were recording internal energy of incoming light, then the performance ratio of PV systems must have been considerably lower during overcast days. However, reports are not showing such evidence.*

[4] *The type of radiation sources might be different in laboratories. Luminescence and thermal radiations emit light based on different physical phenomena, and thereby, they have different shares of entropy* per *wavelength. Nevertheless, this does not make an influence when comparing solar cells even with different material technologies in the lab because the light sources provide the same exergy spectrum which is calibrated by the same device or procedure.*

PV systems. Since direct and diffuse components of the sunlight spectrum have different shares of entropy and consequently have different quality factors, they have different weights. Usually, the tilt angle that maximizes the G_{PoA} equation is theoretically selected for optimum tilt (in real PV installation other considerations also influence the final tilt selection such as wind load, ground coverage ratio, and aesthetical aspects): $G^{E}_{PoA} = G^{E}_{Beam} + G^{E}_{Diffuse} + G^{E}_{Albedo}$. Thus, the tilt angle that leads to the highest energy for G_{PoA} is selected. However, the tilt angle that leads to the highest exergy of impinging radiation must be selected. Therefore, here we suggest the following equation for the tilt optimization of the PV systems: $G^{Ex}_{PoA} = q_b\ G^{E}_{Beam} + q_d\ [G^{E}_{Diffuse} + G^{E}_{Albedo}]$, q_b and q_d are respectively radiation quality factors for beam and diffuse components of sunlight as discussed in Sections 2.1 and 3.1. Since $q_b > q_d$, the effect of such tilt modification will be more visible in the areas with a high share of diffuse components (e.g. central and northern Europe). We note that irradiation terms in the above equations are functions of wavelength $G(\lambda)$ and thereby beam and diffuse quality factors are also spectrally dependent: $q_b(\lambda)$ and $q_d(\lambda)$. Since PV cells have different spectral responses, the overall effect of the quality factors will be different for different PV technologies. Using the spectral response function of PV technologies $SR(\lambda)$, we can separately define the effective radiation quality factor q_{eff} for beam and diffuse components ($q_{eff\text{-}b}$ and $q_{eff\text{-}d}$) corresponding to each PV technology as follows:

$$q_{eff} = \frac{\int Ex(\lambda)SR(\lambda)d\lambda}{\int U(\lambda)SR(\lambda)d\lambda} \tag{17}$$

Table 2 shows q_{eff} values for several PV technologies. As can be seen, $q_{eff\text{-}b}$ and $q_{eff\text{-}d}$ are the highest for amorphous silicon and the lowest for crystalline silicon. In other words, the entropy content of terrestrial radiation has the least influence on amorphous silicon technology while its effect is maximized for crystalline silicon. Therefore, when optimizing a PV system tilt, neglecting the difference in entropy share of direct and diffuse radiations makes more impact when c-Si technology is installed, which dominates the PV market. This signifies the importance of entropy in global energy production.

We note that when G_{Beam}, $G_{Diffuse}$, and G_{Albedo} values are from in-filed measurements, they are already indicating exergy values (G^{Ex}) and the aforementioned tilt optimization method shall not be applied. Nevertheless, in several calculations for tilt optimization, the values are from physical or numerical decomposition and transposition models [65,66], which are indicating energy (G^{E}).

4.4. PV system yield simulation

Another application of this study is the influence of entropy on the accuracy of PV electrical yield simulation and forecasting. As PV is spreading, more research- and commercial-based software tools are being developed for PV forecasting [68,69] and some are also used to guarantee the output electrical yield of PV systems through insurance contracts [70]. However, neglecting the entropy content of sunlight might cause an overestimation in yield predictions. In yield prediction methods, usually predicted or measured GHI is used as an initial point for simulation (only GHI is often measured at meteorological stations). Further GHI is broken into DNI and DHI components through irradiance decomposition models and further used in yield calculation processes. However, the inaccuracy happens because equal importance is given to both direct and diffuse components while they have different radiation qualities. Since the sunlight spectrum and share of direct and diffuse lights changes spatially and temporarily, one can calculate the deviation in yield prediction as a result of neglecting entropy globally. This could lead to entropy-based geographically oriented PV cell and system designs. Despite the interests it raises, it is outside the scope of the current paper.

Table 2
Effective radiation quality factors of beam AM 1.5 ($q_{eff\text{-}b}$), diffuse AM1.5 ($q_{eff\text{-}d}$), global AM1.5 ($q_{eff\text{-}g}$), and blackbody 5800 K ($q_{eff\text{-}o}$) for various PV technologies. The spectral response curves were obtained by digitizing the $SR(\lambda) = (q\lambda/hc)\,EQE(\lambda)$ graphs from Ref. [67].

Technology	$q_{eff\text{-}b}$ (%)	$q_{eff\text{-}d}$ (%)	$q_{eff\text{-}g}$ (%)	$q_{eff\text{-}o}$ (%)
aSi:H	93.94	81.06	92.46	94.24
CdTe	93.81	78.95	92.06	94.09
c-Si	93.60	78.03	91.66	93.93
CZTSS	93.85	79.66	92.19	94.14
GaAs	93.80	79.48	92.04	94.11
mc-Si	93.60	77.93	91.67	94.20
Organic	93.88	80.66	92.27	93.93

4.5. PV system standards

Another application of this work is that it influences PV system standards, especially those related to cabling and fuse rating (Ampacity). The general recommendation by well-known IEC, NEC, IEEE, and UL standards is to size PV system DC cables based on $1.56 \times J_{SC}$ rule, in which 1.56 consists of two factors of $N = 1.25$ and $E = 1.25$ [71–73]. N and E factors respectively represent normal operation and equipment limitation. Normal operation is unique to PV systems, as they are working under outdoor condition and their output current can increase as a result of temperature and irradiance variations. Now that it is shown that the output current of PV systems is influenced by the radiation quality factor, therefore the N factor reduces to $1.25 \times q_{eff}$, and eventually, the sizing factor reduces to $1.56 \times q_{eff} \times J_{SC}$, which is for c-Si is equal to $1.43 \times J_{SC}$. In this way, unnecessary cable oversizing and costs can be avoided for PV systems.

5. Summary

The motivation behind this study was to draw the attention of the PV community to the importance of incoming thermal radiation entropy and its implications. This was pursued by calculating outdoor terrestrial efficiency limits for single-junction crystalline silicon PV technology, with and without considering non-radiative recombination. It was shown that for single-junction silicon solar cells, considering entropy of the incoming radiation reduces the already established laboratory efficiency limit and optimum thickness to 27.12% and ~101 μm, respectively. The study influences optimal PV device design, simulation, and yield prediction. The implications extend to PV system optimal tilt and cabling standards as well.

CRediT authorship contribution statement

Hesan Ziar: Writing – review & editing, Writing – original draft, Visualization, Validation, Supervision, Software, Resources, Methodology, Investigation, Formal analysis, Data curation, Conceptualization.

Declaration of competing interest

The authors declare that they have no known competing financial interests or personal relationships that could have appeared to influence the work reported in this paper.

References

[1] M. Planck, On the theory of the energy distribution law of the normal spectrum, J Verh. Deut. Phys. Ges 2 (1900) 237–245.
[2] P. Wurfel, Wuerfel–Physics of Solar Cells–From Principles to New Concepts, Wiley-VCH, 2005.
[3] A.H. Smets, et al., Solar Energy: the Physics and Engineering of Photovoltaic Conversion, Technologies and Systems, UIT Cambridge, 2015.
[4] M.A. Green, Third Generation Photovoltaics: Advance Solar Energy Conversion, Springer, 2006.

[5] E. Sciubba, W. Göran, A brief commented history of exergy from the beginnings to 2004, Int. J. Therm. 10 (1) (2007) 1–26.
[6] H.D. Baehr, S. Kabelac, Thermodynamik, vol. 12, Springer, 1966.
[7] L.-S. Wang, A Treatise of Heat and Energy, Springer, 2020.
[8] R. Petela, Exergy of heat radiation, J. Heat Tran., Trans. ASME (1964) 187–192.
[9] W.H. Press, Theoretical maximum for energy from direct and diffuse sunlight, Nature 264 (5588) (1976) 734–735.
[10] P. Landsberg, J. Mallinson, Thermodynamic constraints, effective temperatures and solar cells, in: International Conference on Solar Electricity, 1976.
[11] Y. Candau, On the exergy of radiation, Sol. Energy 75 (3) (2003) 241–247.
[12] S.X. Chu, L.H. Liu, Analysis of terrestrial solar radiation exergy, Sol. Energy 83 (8) (2009) 1390–1404.
[13] T. Markvart, G.H. Bauer, What is the useful energy of a photon? Appl. Phys. Lett. 101 (19) (2012), 193901.
[14] A.D. Kirwan Jr., Intrinsic photon entropy? The darkside of light, Int. J. Eng. Sci. 42 (7) (2004) 725–734.
[15] A. Delgado-Bonal, Entropy of radiation: the unseen side of light, Sci. Rep. 7 (1) (2017) 1–11.
[16] P. Baruch, et al., On some thermodynamic aspects of photovoltaic solar energy conversion. 36 (2) (1995) 201–222.
[17] W. Shockley, H.J. Queisser, Detailed balance limit of efficiency of p-n junction solar cells, J. Appl. Phys. 32 (3) (1961) 510–519.
[18] Photovoltaic Report, Fraunhofer Institute for Solar Energy Systems, ISE, 2020.
[19] T. Tiedje, et al., Limiting efficiency of silicon solar cells. 31 (5) (1984) 711–716.
[20] L. Meitner, Über die entstehung der β-strahl-spektren radioaktiver substanzen, Z. Phys. 9 (1) (1922) 131–144.
[21] P. Auger, Sur les rayons β secondaires produits dans un gaz par des rayons X, CR Acad. Sci.(F) 177 (1923) 169.
[22] R. Sietmann, False attribution, Phys. Bull. 39 (8) (1988) 316.
[23] D. Matsakis, et al., A renaming proposal:"The Auger-Meitner effect'. 72 (9) (2019) 10–11.
[24] M.J. Kerr, et al., Limiting efficiency of crystalline silicon solar cells due to Coulomb-enhanced Auger recombination. 11 (2) (2003) 97–104.
[25] A. Richter, M. Hermle, S.W. Glunz, Reassessment of the limiting efficiency for crystalline silicon solar cells, IEEE J. Photovolt. 3 (4) (2013) 1184–1191.
[26] P. Wurfel, The chemical potential of radiation, Solid State Phys. 15 (18) (1982) 3967.
[27] A. Standard, G173-03-Standard Tables for reference solar spectral irradiances: direct Normal and Hemispherical on 37 tilted surface, Annu. Book ASTM Stand. (2003) 14, 2012.
[28] C.A. Gueymard, SMARTS code, Version 2.9, 5 User's Manual. Solar Consulting Services (2005). Available from http://www.solarconsultingservices.com/SMARTS295_manual.pdf.
[29] S. Rühle, Tabulated values of the Shockley–Queisser limit for single junction solar cells, Sol. Energy 130 (2016) 139–147.
[30] T. Kirchartz, U. Rau, Detailed balance and reciprocity in solar cells, Phys. Status Solidi 205 (12) (2008) 2737–2751.
[31] G. Kirchhoff, On the relation between the radiating and absorbing powers of different bodies for light and heat, Lond. Edinb. Dublin Philos. Mag. J. Sci. 20 (130) (1860) 1–21.
[32] A. Polman, H.A. Atwater, Photonic design principles for ultrahigh-efficiency photovoltaics, Nat. Mater. 11 (3) (2012) 174–177.
[33] M.A. Green, Limits on the open-circuit voltage and efficiency of silicon solar cells imposed by intrinsic Auger processes, IEEE Trans. Electron Devices 31 (5) (1984) 671–678.
[34] M.A. Green, Limiting efficiency of bulk and thin-film silicon solar cells in the presence of surface recombination, Progr. Photovolt.: Res. Appl. 7 (4) (1999) 327–330.
[35] K.R. McIntosh, P.P. Altermatt, A freeware 1D emitter model for silicon solar cells, in: 2010 35th IEEE Photovoltaic Specialists Conference, IEEE, 2010.
[36] G.L. Pearson, J. Bardeen, Electrical properties of pure silicon and silicon alloys containing boron and phosphorus, Phys. Rev. 75 (5) (1949) 865.
[37] P. Altermatt, A. Schenk, G. Heiser, A simulation model for the density of states and for incomplete ionization in crystalline silicon. I, *Establishing the model in Si: P.* Journal of Applied Physics 100 (11) (2006), 113715.
[38] P. Altermatt, et al., A simulation model for the density of states and for incomplete ionization in crystalline silicon. II, *Investigation of Si:As and Si:B and usage in device simulation.* Journal of Applied Physics 100 (11) (2006), 113715.
[39] A. Schenk, Finite-temperature full random-phase approximation model of band gap narrowing for silicon device simulation, J. Appl. Phys. 84 (7) (1998) 3684–3695.
[40] P.P. Altermatt, et al., Numerical modeling of highly doped Si: P emitters based on Fermi–Dirac statistics and self-consistent material parameters, J. Appl. Phys. 92 (6) (2002) 3187–3197.
[41] A. Schenk, Advanced Physical Models for Silicon Device Simulation, Springer-Verlag Wien, 1998.
[42] W. Ehrenberg, The electric conductivity of simple semiconductors, Proc. Phys. Soc. Sect. A 63 (1) (1950) 75.
[43] T. Fukushima, Precise and fast computation of inverse Fermi–Dirac integral of order 1/2 by minimax rational function approximation, Appl. Math. Comput. 259 (2015) 698–707.
[44] A. Richter, et al., Improved quantitative description of Auger recombination in crystalline silicon, Phys. Rev. B 86 (16) (2012), 165202.
[45] T. Trupke, et al., Temperature dependence of the radiative recombination coefficient of intrinsic crystalline silicon, J. Appl. Phys. 94 (8) (2003) 4930–4937.
[46] P.P. Altermatt, et al., Injection dependence of spontaneous radiative recombination in c-Si: experiment, theoretical analysis, and simulation, in: NUSOD'05. Proceedings of the 5th International Conference on Numerical Simulation of Optoelectronic Devices, 2005, IEEE, 2005.
[47] M.A. Green, Self-consistent optical parameters of intrinsic silicon at 300 K including temperature coefficients, Sol. Energy Mater. Sol. Cells 92 (11) (2008) 1305–1310.
[48] M. Rüdiger, et al., Parameterization of free carrier absorption in highly doped silicon for solar cells, IEEE Trans. Electron Devices 60 (7) (2013) 2156–2163.
[49] M.A. Green, Silicon Solar Cells: Advanced Principles & Practice, Centre for Photovoltaic Devices and Systems, 1995.
[50] N.D. Arora, J.R. Hauser, D.J. Roulston, Electron and hole mobilities in silicon as a function of concentration and temperature, IEEE Trans. Electron Devices 29 (2) (1982) 292–295.
[51] M.A. Green, et al., Solar cell efficiency tables (version 56), Progr. Photovolt.: Res. Appl. 28 (7) (2020) 629–638.
[52] M.A. Green, et al., Solar cell efficiency tables (version 41), Progr. Photovolt.: Res. Appl. 21 (1) (2013) 1–11.
[53] Green, et al., Solar cell efficiency tables (version 45), Progr. Photovolt.: Res. Appl. 23 (1) (2015) 9, 1.
[54] M.A. Green, et al., Solar cell efficiency tables (version 50), Progr. Photovolt.: Res. Appl. 25 (7) (2017) 668–676.
[55] M.A. Green, et al., Solar cell efficiency tables (version 53), Progr. Photovolt.: Res. Appl. 27 (2018) 3–12.
[56] M.A. Green, et al., Solar cell efficiency tables (version 54), Progr. Photovolt.: Res. Appl. 27 (2019) 565–575.
[57] M.A. Green, et al., Solar cell efficiency tables (Version 55), Progr. Photovolt.: Res. Appl. 28 (1) (2020) 3–15.
[58] P.K. Nayak, et al., Photovoltaic solar cell technologies: analysing the state of the art, Nat. Rev. Mater. 4 (4) (2019) 269–285.
[59] PVlighthouse, cited 2021; Available from, https://www.pvlighthouse.com.au/.
[60] W. Wang, Simulate a 'Sun' for Solar Research: A Literature Review of Solar Simulator Technology, Literature review in Royal Institute of Technology Stockholm, Sweden, 2014, pp. 1–37.
[61] S.H. Jang, M.W. Shin, Fabrication and thermal optimization of LED solar cell simulator, Curr. Appl. Phys. 10 (3) (2010) S537–S539.
[62] R. Rösemann, C. Lee, in: Kipp, Zonen (Eds.), A Guide to Solar Radiation Measurement: from Sensor to Application: an Overview of the State of the Art: UV, Visible, Infrared, 2011.
[63] R. Dabou, et al., Monitoring and performance analysis of grid connected photovoltaic under different climatic conditions in south Algeria, Energy Convers. Manag. 130 (2016) 200–206.
[64] M. Singh, et al., Comparing optical performance of a wide range of perovskite/silicon tandem architectures under real-world conditions, Nanophotonics 10 (8) (2021) 2043–2057.
[65] B. Ridley, J. Boland, P. Lauret, Modelling of diffuse solar fraction with multiple predictors, Renew. Energy 35 (2) (2010) 478–483.
[66] R. Perez, et al., Modeling daylight availability and irradiance components from direct and global irradiance, Sol. Energy 44 (5) (1990) 271–289.
[67] M. Brennan, et al., Effects of spectral albedo on solar photovoltaic devices, Sol. Energy Mater. Sol. Cell. 124 (2014) 111–116.
[68] Comprehensive PV systems modelling toolbox [cited 2021; Available from, *https://www.tudelft.nl/solarurban/research/projects/comprehensive-pv-systems-modelling-toolbox*.
[69] PVsyst, Available from, *https://www.pvsyst.com/*, 2021.
[70] Solar mokey, Available from, *https://solarmonkey.io/*, 2021.
[71] National Electrical Code, Article 690—Solar Photovoltaic Systems, NFPA, Quincy, MA, USA, 2011.
[72] Electrical Installations of Buildings—Part 7-712: Requirements for Special Installations or Locations—Solar Photovoltaic Power Supply Systems, IEC 60364-7-712 (2002).
[73] IEEE Guide for Terrestrial Photovoltaic Power System Safety, IEEE Std., Sep. 1998, p. 1374.